Available online at www.sciencedirect.com

ScienceDirect

journal homepage: www.elsevier.com/locate/he

Quantitative hydrogen and methane gas sensing via implementing AI based spectral analysis of plasma discharge

Ali Salimian

Department of Computer Science, School of Engineering, London Southbank University, 103 Borough Road, London SE1 0AA, UK

HIGHLIGHTS

- A hydrogen detection system is proposed, and a prototype constructed by modifying a small bench top RF plasma system.
- The plasma sustemr is coupled to a spectrophotometer for capturing spectral data of the plasma as data.
- Spectral data associated with different target gas quantities in the plasma are collected to train a deep learning model.
- The plasma system and the trained model can act as hydrogen quantification conceptual system which is evaluated here.

ARTICLE INFO

Article history:
Received 9 August 2023
Received in revised form
15 September 2023
Accepted 2 October 2023
Available online 17 October 2023

Keywords:
Hydrogen
Plasma
Detectors
Computer Vision
Deep Learning
Neural Networks

ABSTRACT

In this report we explore the feasibility of a quantitative gas detection system concept based on alternations in spectral emissions of a radio frequency power generated plasma in presence of a target gas. We then proceed with training a deep learning residual network computer vison model with the spectral data obtained from the plasma to be able to perform regressive calculation of the target gas content in the plasma. We explore this concept with hydrogen and methane gas present in the plasma at know quantities to evaluate the applicability of the concept as hydrogen or methane detection system. We will demonstrate that the system is well capable of quantitatively detecting either of the gases efficiently while it is challenging to estimate hydrogen content in presence of methane.

1. Introduction

The present situation of industrial expansion, alongside a significant increase in population, necessitates a substantial demand for energy. This requirement must be fulfilled by a combination of traditional and renewable energy sources. Undoubtedly, sustainable energy sources have served as the cornerstone for numerous recent advancements in science and technology, but the walk from fossil fuels to renewables such as tidal, solar and wind will trail through a bumpy ride due to the well know limitations associated with their implementation.

Hydrogen, however, can be an ideal substitute for a world currently so used to thrive on a fossil fuel diet. As an illustration, hydrogen boasts an impressive energy density of 120 MJ/kg, which is roughly three times higher than that of gasoline and diesel fuels. In electrical terms, each kilogram of hydrogen contains 33.6 kWh of useable energy (in fuel cell),

E-mail address: salimiaa@lsbu.ac.uk.
https://doi.org/10.1016/j.ijhydene.2023.10.010

while a comparable amount of diesel fuel provides about 12–14 kWh/kg. To put this into further context, lithium-ion batteries, which are considered a high-quality rechargeable battery technology with advantages over nickel-cadmium (Ni–Cd) or nickel-metal-hydride (Ni-MH) batteries, have an energy density of approximately 0.2 kWh/kg [1].

A crucial point to note is that hydrogen can also serve as a fuel in a fuel cell, which exhibits high efficiency in producing electricity [2]. This exciting prospect opens new opportunities for car manufacturers [3].

But let's tread carefully, firstly, there are two primary types of hydrogen: "grey" hydrogen and "green" hydrogen. Grey hydrogen is produced using fossil fuels, such as natural gas, and it releases greenhouse gases during its production process. On the other hand, green hydrogen is generated without emissions by utilising renewable energy sources like solar and wind energy. "Green hydrogen" is considered the most promising form of hydrogen for the future since it has the potential to reduce greenhouse gas emissions and mitigate the effects of climate change. However, the current manufacturing process for green hydrogen remains expensive, making it crucial to explore more efficient and cost-effective methods of production [4].

Secondly, while hydrogen assisted mankind to step on the moon by thrusting the Saturn V rocket, it also caused the Hindenburg airship disaster on may 6, 1937. The safety concerns surrounding hydrogen-based technologies is of utmost importance due to hydrogen's flammability across a broad range of concentrations in air (4–75%). Moreover, it becomes explosive within a wide range of concentrations (15–59%) at standard atmospheric temperatures [5]. In practical terms, if there is a hydrogen leak in an enclosed space, it is highly probable that an explosion rather than just a simple flame will occur. This characteristic of hydrogen makes its utilization especially hazardous in confined areas, such as tunnels and underground parking facilities. Special precautions and safety measures are essential when dealing with hydrogen in such environments to mitigate potential risks. So, we need instruments to sense hydrogen leaks. The essential requirements for a dependable hydrogen gas sensor can be summarized as follows [6].

i. The sensor should be capable of indicating low to moderate levels of gas concentrations, ranging from 0.01% to 10%.
ii. Precise and accurate detection of gases should be ensured by the sensor.
iii. Minimum interference from humidity and other gases should be observed.
iv. The sensor should perform effectively under unfavourable operating conditions, including high pressure, temperature, and gas flow rates.
v. The signal produced by the sensor should exhibit low overall noise.
vi. Fast response and recovery times are essential, aiming for less than 5 s.
vii. The fabrication and maintenance costs of the sensor should be kept low.
viii. The sensor should be designed to be small and compact, allowing for ease of installation and use.

1.1. *The existing sensing technologies*

There are many techniques implemented for hydrogen detection, each utilising a particular property or properties of materials and their interactions in absence or presence of hydrogen. These technologies are illustrated in Fig. 1 and discussed briefly.

Work function method: The minimum amount of energy, measured in electron volts (eV), needed to remove an electron from the surface of a metal and send it to infinity is referred to as a work function. In hydrogen sensing applications, a metal that is sensitive to hydrogen gas is coated over an oxide layer. When hydrogen gas is present, its atoms diffuse through the metallic layer and get adsorbed at the interlayer between the metal and the oxide. At this stage, the hydrogen atoms become polarized, leading to a change in the work function of the metal. This alteration in the work function can be detected as a voltage change, allowing for the confirmation of the presence of hydrogen gas [7–9].

Optical Method: The optical method of gas sensing relies on detecting changes in the optical properties of specific materials after gas molecules are adsorbed onto them. This technique utilizes an interferometer compatible optical cable and a hydrogen-sensitive metallic coating, typically made of Pd (palladium). As hydrogen gas molecules are adsorbed over the surface of the Pd coating, the reflectivity of the surface undergoes alterations. Here's how the process works: A light beam is transmitted through the optical cable and directed towards the coated surface. Upon reaching the surface, the light interacts with the adsorbed hydrogen gas molecules, causing changes in the reflectivity of the surface. The modified light beam is then received back by the interferometer, where the changes in its reflectivity are observed and correlated to the concentration of hydrogen gas present in the environment. By analysing the variations in reflectivity, this method allows for the detection and measurement of hydrogen gas concentrations in the surroundings [9–16].

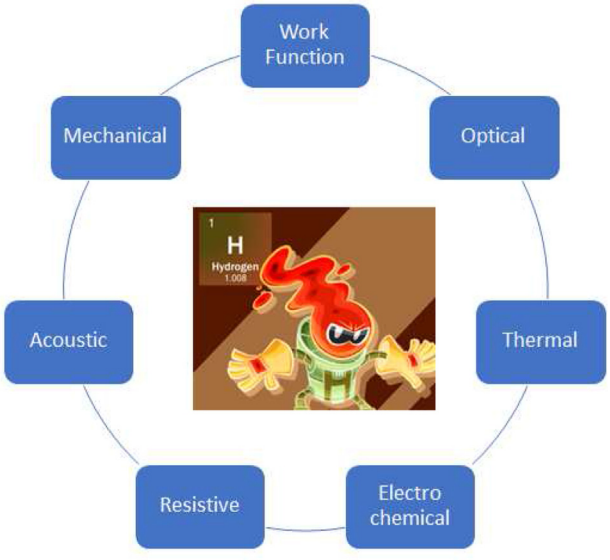

Fig. 1 – Some of the current methods implemented in hydrogen sensing.

Thermal method: The principle behind this method relies on the fact that hydrogen gas has a higher thermal conductivity (0.18 W/mK at 300 K) compared to normal air (0.026 W/mK at 300 K). This property makes it useful for detecting the presence of H2 gas in the air. The operating principle of this method involves measuring the heat loss of a body to the surrounding gas. The extent of heat loss is influenced by the thermal conductivity of the surrounding gas. When more hydrogen gas is introduced into the air, the heat dissipation increases due to the higher thermal conductivity of the medium. To implement this method, two resistors are utilised: one for the reference gas (air) and the other for the target gas (H2). These resistors are connected to a Wheatstone bridge. Under normal conditions, when only air is present in both cells, the resistors lose heat equally, resulting in the same reading. However, when the target gas (H2) enters the respective cell, the heat loss of the target gas resistor differs from the air resistor due to the presence of hydrogen gas (resulting in an increase in heat loss). The imbalance in the Wheatstone bridge caused by this heat loss difference allows for accurate detection of hydrogen gas concentrations in the surrounding environment based on the changes in heat dissipation and resistance imbalance in the Wheatstone bridge [17–20].

Resistive method: Here, metal oxide-based resistive sensors which have variable resistance in presence of hydrogen are utilised. These materials are typically fabricated on a substrate, which can be an insulating material like Al2O3 or SiO2. The sensors consist of multiple layers. First, interdigitated electrodes made of noble metals such as Au, Ag, or Pt are coated onto the insulating layer. On top of these electrodes, a metal oxide layer is applied, forming the sensing element. The resistance across the electrodes coated with the metal oxide sensing element is measured in the presence and absence of H2 gas. By calibrating the difference in resistive load with the ambient gas concentration, hydrogen gas can be detected [21–28].

Acoustic method: In the acoustic method of gas detection, changes in the surface properties of a piezoelectric material, caused by the adsorption of gas molecules, are measured in the form of surface-generated acoustic waves. Various devices can be employed to detect these waves, with one such device being the quartz crystal microbalance (QCM). The QCM consists of a small and thin quartz disc with electrodes printed on each side. When an electric field is applied to the electrodes, it causes deformation in the structure of the quartz disc, leading to its resonance. The resonance frequency of the disc is highly sensitive to the mass of the material on its surface. Thus, when gas molecules in the ambient environment get adsorbed on the coated surface, the mass of the disc changes. This alteration in mass is detected by measuring the change in resonance frequency. The shift in resonance frequency indicates the presence of hydrogen gas in the surrounding environment. By monitoring these changes in resonance, the QCM device can effectively detect the concentration of hydrogen gas with high sensitivity and accuracy [29–35].

Mechanical method: These sensors are based on monitoring the changes in the physical properties of a metal in the presence of hydrogen gas. Typically, a metal sensitive to hydrogen, such as palladium, is coated over a micro cantilever. In the presence of hydrogen gas, gas molecules get adsorbed into the interstitial sites of the metal lattice, causing the micro cantilever to expand. This expansion is observable as deflection or bending of the thin film micro cantilever [36–40].

Electrochemical method: These sensors can be classified as either amperometric or potentiometric, based on the nature of the signal they produce. In an amperometric sensor, a constant voltage is applied, and the sensor measures the diffused current resulting from the reaction between the target gas (hydrogen) and the sensing material. The sensor typically consists of three electrodes: the sensing electrode, the counter electrode, and the reference electrode. The sensing electrode is made of a material suitable for the oxidation of hydrogen gas, and it is where the gas reacts and undergoes an electrochemical process. The counter electrode's role is to provide a path for the current to flow back to the sensor circuit, completing the electrical circuit. The reference electrode maintains a stable and known potential against which the potential of the sensing electrode is measured. By measuring the current flow between the sensing and counter electrodes at a constant voltage, the sensor can determine the concentration of hydrogen gas in the environment [41–46].

Chauhan et al. have produced a great review on hydrogen sensing techniques for detailed description of existing technologies [47]. However, the disadvantage of the techniques discussed is summarized in Fig. 2.

1.2. *Alternative concept*

Here we report on some preliminary experiments on hydrogen detection via spectral analysis of a plasma of air containing hydrogen. We implement artificial intelligence (AI) based spectral analysis of the plasma generated with known quantities of hydrogen content and use the spectral data to train a deep learning model that can extract features from the plasma emissions and associate them to the precise hydrogen levels present in the plasma. Such an algorithm coupled to the hardware can act as a reliable hydrogen purity analyser or leak detector. We also do look into the application of this technique for methane quantification.

1.3. *Hydrogen plasma*

Hydrogen plasma bands and emission peaks refer to the specific spectral lines and bands of light emitted or absorbed by hydrogen in a plasma state. A plasma is an ionized gas in which the atoms are split into charged particles, such as electrons and ions. When hydrogen is in a plasma state, it can emit light as the electrons transition between different energy levels. In the context of hydrogen plasma, there are several prominent spectral lines and bands that are of particular interest (48–50):

Balmer Series: The Balmer series is a set of spectral lines corresponding to the transitions of electrons in hydrogen atoms from higher energy levels to the second energy level ($n = 2$). These transitions result in the emission of visible light. The Balmer series includes several lines, with the most prominent ones occurring in the visible region of the

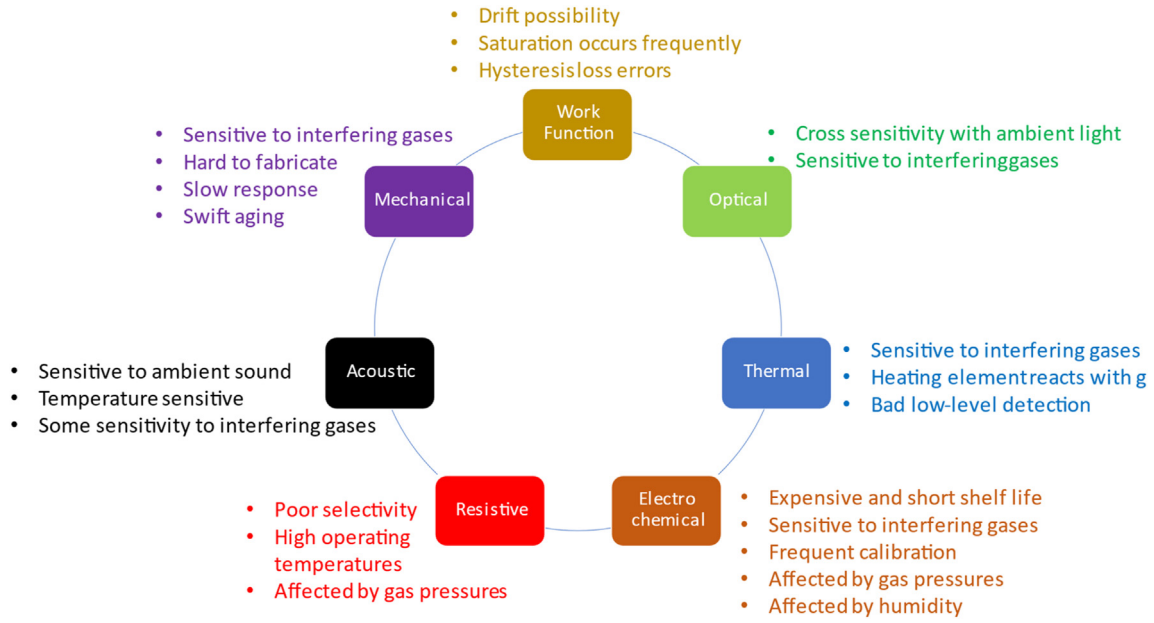

Fig. 2 – The main draw backs of the existing hydrogen sensing systems.

electromagnetic spectrum, such as H-alpha (656.3 nm), H-beta (486.1 nm), H-gamma (434.1 nm), and so on.

Lyman Series: The Lyman series represents spectral lines that occur when electrons in hydrogen atoms transition from higher energy levels to the first energy level (n = 1). These transitions typically result in the emission of ultraviolet (UV) light. The most well-known line in the Lyman series is the Lyman-alpha line (121.6 nm).

Paschen Series: The Paschen series corresponds to the transitions of electrons in hydrogen atoms from higher energy levels to the third energy level (n = 3). The emitted light is generally in the infrared (IR) region. The most prominent line in the Paschen series is Paschen-alpha (1875.1 nm).

Brackett Series: The Brackett series involves transitions of electrons from higher energy levels to the fourth energy level (n = 4). This results in the emission of infrared light. The most notable line in the Brackett series is Brackett-alpha (4.05 μm).

These emission peaks and bands play a crucial role in spectroscopy and astrophysics, as they provide valuable information about the energy levels and electronic structure of hydrogen atoms in plasma. By studying the specific wavelengths of light emitted or absorbed, researchers can gain insights into the physical conditions of the hydrogen plasma and its surroundings, including temperature, density, and ionization states. As such, our proposed hydrogen detection concept relies in utilising such emission information from a hydrogen present in an air plasma to quantify the hydrogen content. However, in our experiments the plasma is generated using the ambient air, which includes oxygen, nitrogen, carbon dioxide, moisture and basically any gas present in the air. As such, when low amount of hydrogen is present in such plasma, the associated peaks will not be apparent to the naked eye. However, thanks to the modern computing powers and advanced deep learning algorithms possible with it, we can produce models capable of extracting such hidden information and here we will explore the potential of this approach.

2. Experimental

2.1. *Hardware and instrumental setup*

The experiments were carried out by utilising a bench top radio frequency (RF) plasma cleaner system with a slightly modified chamber door mounted with a collimator that could capture the spectral data from the plasma in the chamber and feed it through an optical fibre into a high-resolution spectrometer. By varying the plasma power and the hydrogen gas fed through a mass flow controller (MFC) into the chamber, numerous plasma conditions were created, and spectral data associated with the plasma were recorded.

The system was set to generate an RF plasma at 30, 40, 60, 80, 100, 120 and 150 W of RF power. The main motive for examining different plasma powers was to examine the impact of power on specific hydrogen lines. Such hydrogen lines will ultimately create features in the data that will enable deep learning models to get trained with data. The system had three MFC intake ports, one was exposed to ambient atmosphere without an adjustment to moisture levels. The other two MFC ports were connected to a pure hydrogen and pure methane source. The MFC controller allowing ambient air was kept at a constant ~40sccm of ambient air input, while the amount of hydrogen allowed into the chamber via the second MFC ranged from 0 to 2 sccm at 0.1 intervals, as such allowing a hydrogen content of between 0 and 5% inside the chamber. For each plasma condition, a total of 20 spectral readings were taken.

The spectrometer was capable of capturing plasma emission peaks from 195 nm to 1105 nm at 0.2 nm resolution. Overall, a total of 2863 spectral plots were captured with each spectrum containing 4550 data points. The system setup is illustrated in Fig. 3. There are certain fine-tuning parameters associated with the RF plasma in these experiments that the

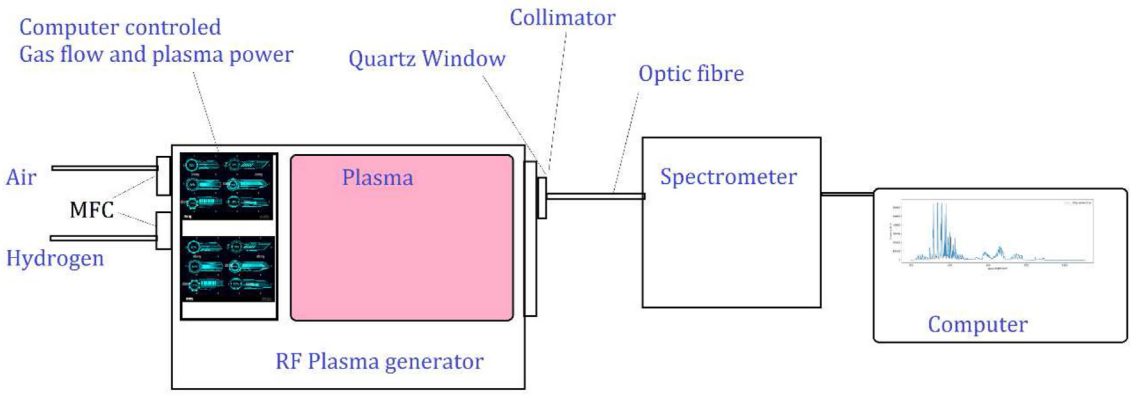

Fig. 3 – The system setup for collecting spectral data of air plasma with known hydrogen impurity.

author cannot disclose for commercial purposes associated with this project.

As we intended to use computer vision based deep learning models (convolutional neural network structures), each single spectrum resembling a vector of 4550 data points was trimmed to only cover emission peaks starting at 200 nm and ending at 1099.8 nm (containing 4500 data points). Such vector will easily contain any information associated with the Balmer series discussed earlier as well as many other possible emission peaks associated with hydrogen.

2.2. *Data collection and processing*

The trimmed vector was then converted into a 50 by 90 matrix, by stacking every 50 data points of the trimmed vector on top of each other. As such, each of the 2863 spectral data were converted into a matrix bearing 50 rows and 90 columns. This step is graphically illustrated in Figs. 4 and 5. We could now treat the spectrum as an image. These images will act as our image data for training a convolutional neural network model with a regressor output.

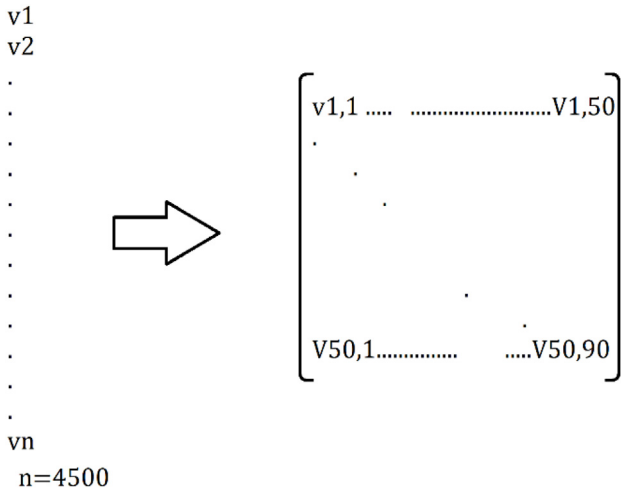

Fig. 4 – Conversion of the single array of emission peaks in to a 2D matrix array. As such the spectral data is converted into an image form suitable for training computer vision models.

When looked at with a naked eye, it is literally impossible to distinguish such images when associated with different hydrogen content. For example, 2D spectral images associated with hydrogen content of 0.26% and 1.03% are presented in Fig. 6. The standard spectra of the two plasma conditions to the naked eye look extremely similar and so do the 2D images derived from them.

Similar experiments and data collections were carried out with an air plasma containing methane impurity. These experiments exactly mimic the hydrogen sensing protocols except that data were only collected at 120w rather than using various RF plasma power outputs. The 120w RF power output was selected given the better performance of 120w plasma power for hydrogen sensing which will be discussed in the next sections. In these experiments along with hydrogen some various quantities of methane were admitted into the chamber precisely through a MFC inlet.

3. Modelling

Convolutional Neural Networks (CNNs) are a class of deep learning models primarily designed to process and analyse visual data, such as images and videos. CNNs use convolutional layers to automatically learn and extract relevant features from the input image data in form of 2D tensors. This process enables CNNs to perform tasks like image recognition, object detection, and image segmentation, among others.

At its core, the CNN process constitutes:

Input Layer: The input layer receives the raw data, in the form of images (2D tensors). Each image is represented as a grid of pixels, where each pixel corresponds to a specific intensity value.

Convolutional Layers: The core building blocks of CNNs are convolutional layers. Each convolutional layer consists of multiple filters (also known as kernels), which are small windows that slide over the input image. The filters learn to detect different patterns, such as edges, textures, or other visual features, by convolving (element-wise multiplication and summing) with the input image. The result is a feature map that highlights the presence of specific patterns in the input 2D tensor.

Activation Function: After convolution, an activation function, commonly the Rectified Linear Unit (ReLU), is

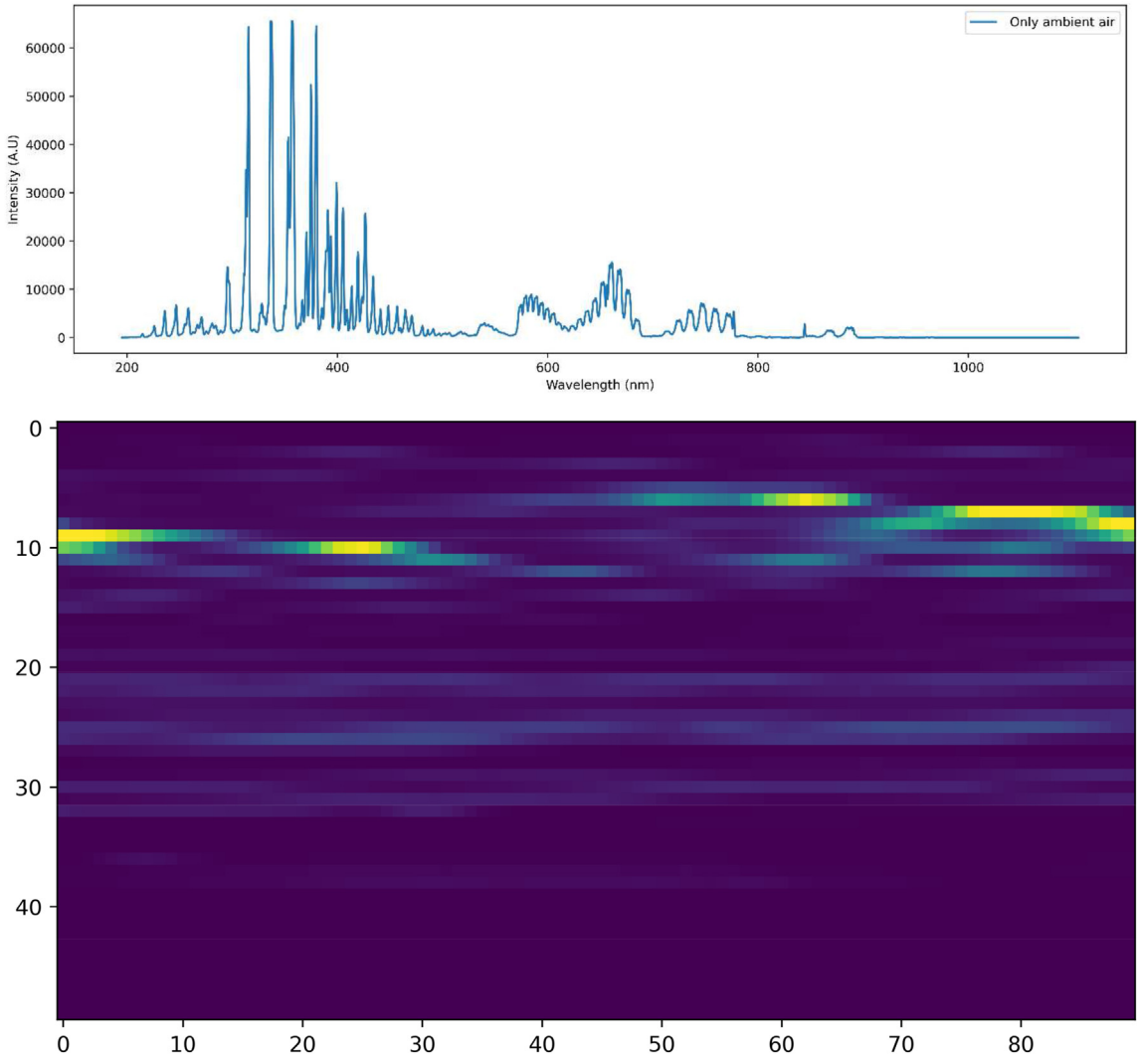

Fig. 5 – Here as an example, a spectral data (top) is converted into a 2D matrix and visualised as an image (bottom). Such image associated with a know hydrogen content is then used to train a computer vision model with a regressive output to predict hydrogen content from such images.

applied elementwise to introduce non-linearity into the network. This allows the CNN to learn more complex and abstract features from the data.

Pooling Layers: Pooling layers follow the convolutional layers to reduce the spatial dimensions of the feature maps. Max pooling is a commonly used technique, where the maximum value within a small window is selected and the rest are discarded. This down sampling helps to reduce the number of parameters, control overfitting, and make the network more computationally efficient.

Fully Connected Layers: After several convolutional and pooling layers, the output is flattened and fed into fully connected layers, which act as a traditional neural network. These layers learn to classify and interpret the extracted features into meaningful outputs, such as object categories or image labels.

Output Layer: The final layer produces the predicted output of the CNN, which could be the probabilities of different classes (in case of classification tasks). How ever, in our approach the output layer, is designed to out put a single number which is indeed the percentage of hydrogen or methane present.

Training: During the training process, the CNN learns the optimal values of its parameters (weights and biases) using backpropagation and gradient descent. The model was trained with only 80% of our spectral data chosen randomly by computer. Another 20% of our spectral data was hidden from the model during its training. Once the model was trained, we evaluated its hydrogen concentration predicting power by testing it with the 20% unseen data and comparing the estimated hydrogen content with actual known value for that spectral data.

The convolutional neural network structure discussed above is the most basic vanilla form of the model structure, in our initial studies, we realised that simple models can on occasions produce reasonable predictions, but overall were not stable and the model performance was not accurate. Fig. 7 illustrates the anatomy of such a simple CNN model that we examined.

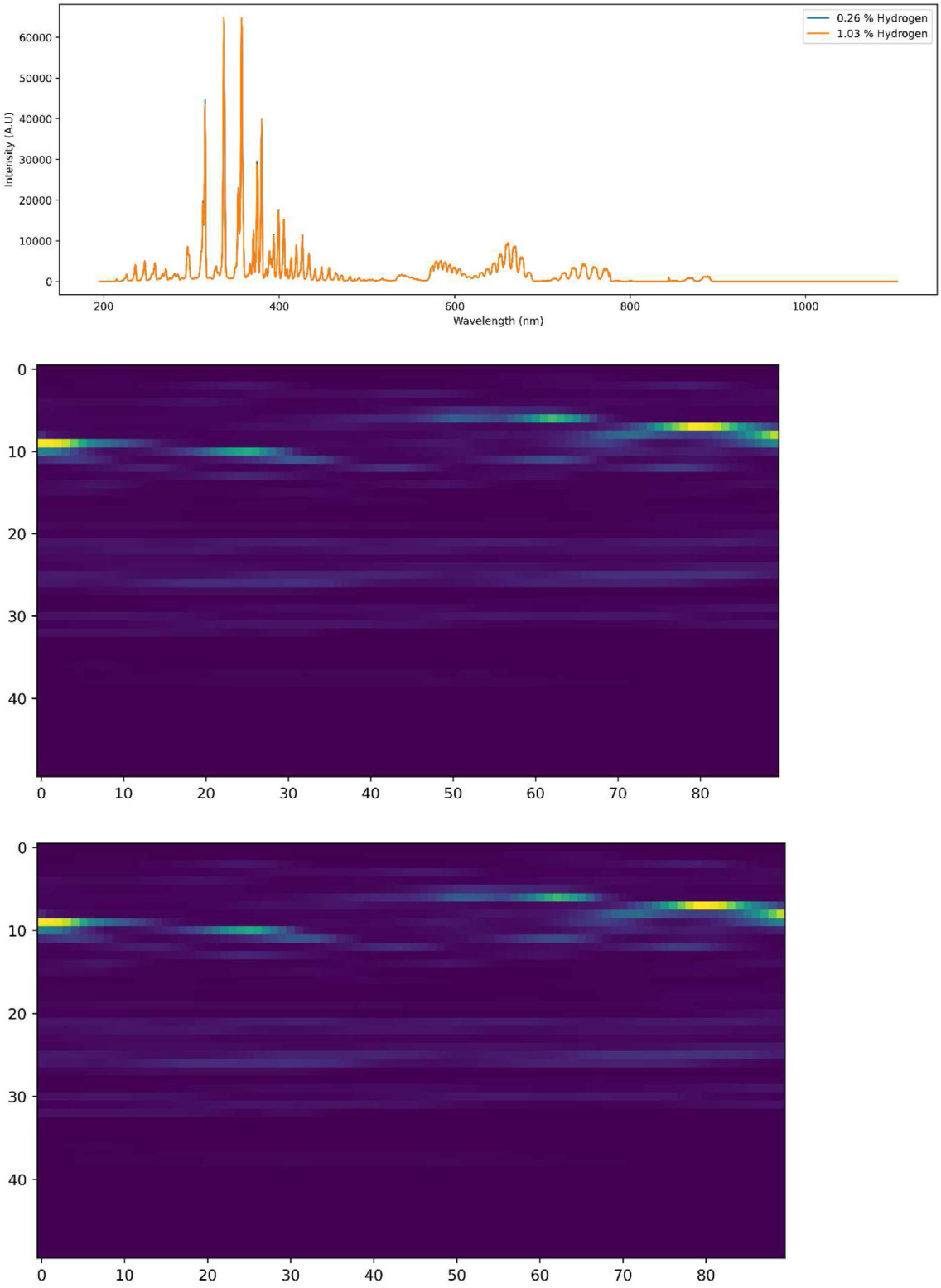

Fig. 6 – An overlap of emission spectra collected for an air plasma containing 0.26% and 1.03% hydrogen (top). The 2D spectral conversion of the 0.26% hydrogen (middle). The 2D spectral conversion of the 0.26% hydrogen (bottom).

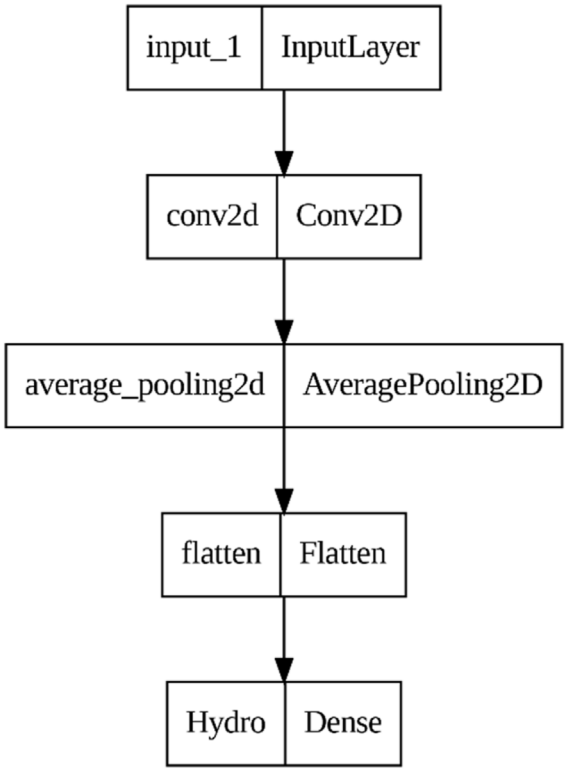

Fig. 7 – The basic structure of a CNN model and the layers of operations involved, starting with an input 2D tensor, convolution process, pooling, flattening and an output dense layer. While such models usually perform good with standard image data for image recognition, the model struggled with calculating hydrogen or methane concentration.

Hence, we structured a significantly more complex CNN model resembling the ResNet v50 residual model structure. In ResNet-50 v2, the residual blocks are organized into different stages. The structure of the residual model is illustrated in Fig. 8. The first stage performs initial convolution and pooling operations, while subsequent stages consist of multiple residual blocks stacked together. The number of residual blocks per stage may vary depending on the architecture variant for better model performance.

Another key feature of the residual model is the use of bottleneck blocks. These blocks are designed to reduce computational complexity by employing 1×1 convolutions to reduce the number of input channels, followed by 3×3 convolutions, and finally 1×1 convolutions to restore the number of channels. This bottleneck design allows the model to achieve better performance with fewer parameters. ResNet-50 v2 has demonstrated excellent generalization capabilities, allowing it to learn hierarchical features that are transferable across different datasets and tasks. Meanwhile, residual models introduce skip connections to CNN network that enable the network to learn residual mappings. These skip connections allow the network to directly learn the difference between the input and the output of a specific layer, rather than trying to learn the entire mapping from scratch. This makes it easier for the network to learn the identity mapping.

4. Results and discussion

The experimental section of the project resulted in spectral data being produced for experiments carried out at 30,40,60,80,100.120 and 150w of plasma power. All the spectra was collected every 1 s, with 50 ms integration time produced averagely by 10 exposures. The basic model and the residual models were trained using these data. As discussed for each experiment, 20% of the data was kept hidden from the model while the model was trained on the 80% of the spectral data points with known hydrogen content.

4.1. *Hydrogen sensing*

As previously mentioned, the basic CNN model was simply unable to learn from the data and performed poorly as can be seen in Fig. 9. As such, all results presented here are associated with training the residual model and the predictions made by the model after training.

The predicted Hydrogen content and real values of the hydrogen at each consecutive plasma power experiments are presented in Figs. 10 and 11. Fig. 10 convers results for spectral data collected with plasma powers under 100w and Fig. 11 presents results associated with above 100w plasma powers. We can see that data generated at different plasma powers influence training and prediction accuracy of the residual models. In particular, the 120w plasma seems to be the optimal method of data collection in this study. This observation can be explained by some studies [48–50] where it was demonstrated that at low plasma powers, only H2 emissions are observed (577 nm–630 nm) while as the RF power further increases the Hα becomes stronger compared to Hβ emissions as well as a prolonged continuum towards 200 nm (A16,A17,A18,A19). Also, the optical emission intensities Iβ, I γ of H β and Hγ linearly increase with the net input power for different energy levels of the excited hydrogen atoms. This can perhaps explain that higher plasma powers can ensure more spectral features become apparent for a computer vision model to utilise them for feature selection from the images.

However, the 150w plasma power to our surprise did not outperform the 120 w set of data in terms of model training. This may be simply due to the fact that ultimately, at 120w plasma power, all the features required from a spectral emission are perfectly sufficient for a deep learning computer vision model to train itself with relevant weights while the 150w may further enhance emissions from other atomic elements present in the plasma (Nitrogen, Oxygen, etc …) that may have a negative effect on feature selection associated with hydrogen emissions. It is widely acknowledged that hydrogen plasma contains a diverse range of particles, including electrons and hydrogen atoms in their ground state, excited hydrogen atoms, hydrogen molecules in their ground state, excited hydrogen molecules, and so on. Among these particles, numerous complex reactions occur, leading to complicated collision

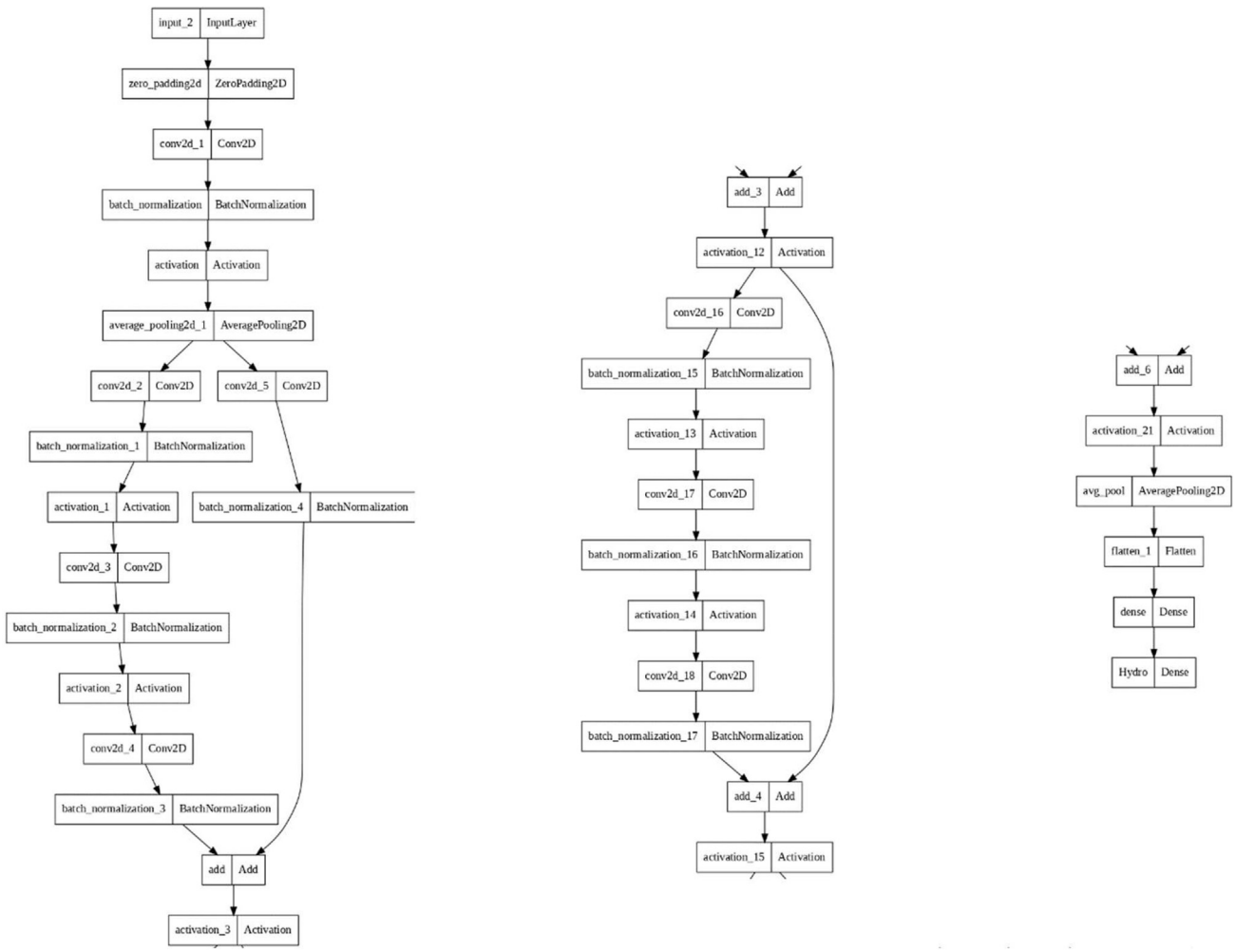

Fig. 8 – The structure of the residual CNN model. The input layer and subsequent convolutional layers are the first stage of the model followed by a residual stage (left). A residual block that follows the first stage, the number of these can be varied to achieve maximum accuracy (centre). The output stage which very much resembles the steps discussed in the vanilla structure of a CNN model (right).

processes between them. The primary generation of excited hydrogen atoms happens through electron impact excitation of H2 molecules or H atoms. Two main methods contribute to this production: dissociation excitation [51] arising from fast electrons colliding with hydrogen molecules, and collision excitation [52] resulting from electrons colliding with hydrogen atoms in their ground state. Consequently, when these excited hydrogen atoms at energy levels $n = 4$ and $n = 5$ transition to the energy level $n = 2$, they emit $H\beta$ and $H\gamma$ emissions [53,54]. However, in our experiments, we also have air (comprised of oxygen, nitrogen, moisture, and other trace gases) present in the plasma which further complicates a detailed discussion on this topic given the scope of our report here, but ultimately, one can argue that further plasma power may lead to signals from such a mix plasma that ultimately overlap features associated with hydrogen emissions.

At this stage, our efforts have been concentrated on demonstrating the concept of a hydrogen detection system based on AI-driven spectral analysis of RF-generated plasma. The results presented thus far offer an intriguing perspective on the potential of this method for hydrogen sensing. Nevertheless, there are additional steps that can be taken to further improve the model's accuracy.

Furthermore, we have delved deeper into the method's capability to assess the presence of methane gas in the plasma, a topic we discuss in the next section.

4.2. *Hydrogen and methane sensing*

The results are interesting when we attempted to train the model with spectral data collected at 120w plasma power with both hydrogen and methane being present the same time. In these experiments spectral data were collected with both hydrogen and methane present at the same time at various quantities in the plasma.

Methane (CH4) plasma has been extensively investigated for many years, making its cross sections the most studied among other gases commonly used in semiconductor

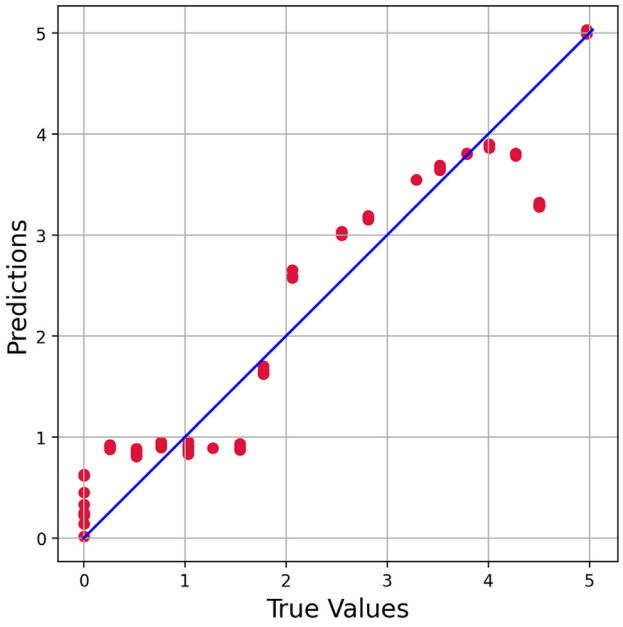

Fig. 9 – Estimation of hydrogen content when a simple model was trained extensively with the data. It is clearly apparent that the model is struggling with precise calculation of the hydrogen content and as such simple models will be redundant for this application.

manufacturing, such as CF4 or SiH4. In a notable study, researchers developed a comprehensive, self-consistent, one-dimensional (1D) simulator to explore the physics and chemistry of radio frequency (RF) plasmas involving CH4. Their model incorporates four key species: CH4, CH3, CH2, and H. The authors made a crucial observation that CH4 plasmas exhibit electropositive behaviour, with negative ion densities approximately one order of magnitude lower than that of electrons. These finding sheds light on the unique characteristics of CH4 plasmas [55–57]. Based on these studies, the primary electron reactions in simple plasma model of hydrogen and methane are presented in Fig. 12.

Once the residual CNN model was trained with spectral data associated with plasma containing both hydrogen and methane, the model was examined by testing it with a set of test spectral data associated with a similar plasma condition to evaluate its accuracy of target gas content. These results are presented in Fig. 13. It can be clearly observed that while the model is fantastically adapted to predict the methane content in the plasma while hydrogen is present there, its performance is significantly undermined for predicting the hydrogen content. The prediction of hydrogen content is extremely inaccurate with large variance indicating that the model is making multiple wrong calculations.

As discussed, and illustrated in Fig. 12, when methane gas is exposed to a high-energy source such as an electric discharge or intense heat, some of the molecules can become ionized, forming ions and free electrons including hydrogen species. These charged particles interact with the surrounding air molecules, leading to various chemical reactions and energy exchanges. While all these exotic ions and chemical reactions occurring in presence of methane are leading to a set of unique emission peaks and regions that are ultimately utilised by the deep learning model for self-training and feature selection associated with methane emissions in plasma, they will also overlap with features associated with hydrogen presence in the plasma. The downside of these new emission characteristics is that they will potentially mask or overlap the unique hidden features which the model was previously utilising to train itself for precise hydrogen content calculations. As such, as it stands despite the impressive performance of the experimental setup in hydrogen detection, it seems to significantly suffer if trying to make hydrogen predictions in presence of methane. As such if a system is required to predict both gases, in its current stage will be unable to perform as such. Hence while the system bears potential as hydrogen detection or methane detection, its quantitative hydrogen sensing will be undermined in presence of methane.

Nevertheless, the results at the same time highlight how powerful the current deep learning computer vision models are. The ResNetv50 model which we have mimicked in this study was originally developed by He et al. for the purpose of image recognition [58]. Just to appreciate how powerful these models are in capturing features, we extracted spectral transition data associated with Hydrogen, Oxygen, Nitrogen and Argon from the National Institute of Standards and Technology (NIST) and converted the wavelengths associated with the transitions into a 2D tensor which is presented in Fig. 14 [59].

Deep learning computer vision models are known to extract hidden features within 2D tensors, by just observing the limited features available from hydrogen and knowing that in our experiments the residual model can detect those features, clearly demonstrates that apart from the feature maps hidden within an image, such models identify intensities at pixel level and can associate it to their neural weights. A plasma with more atomic ingredients will ultimately have numerous signatures on a 2D tensor form which theoretically can be identified by the residual model, however in case of methane, we think the hydrogen species coming off the methane molecule are technically mimicking the exact features associated with the hydrogen alone and as such create a challenge for this concept.

4.3. *Considering the effect of ambient moisture*

As illustrated and discussed, the presence of methane proposes a certain degree of challenge for model training. Methane, comprised of four hydrogen atoms, has the potential to fragment into smaller molecular or atomic units when exposed to a plasma environment (Fig. 12), effectively transforming into hydrogen atoms. As a result, when spectral data is acquired with a controlled flow of hydrogen into the plasma, an undisclosed amount of hydrogen may emerge in the presence of methane, introducing an element of uncertainty. Hydrogen's spectral features exhibit limitations and uniqueness, in contrast to the considerably more intricate spectral

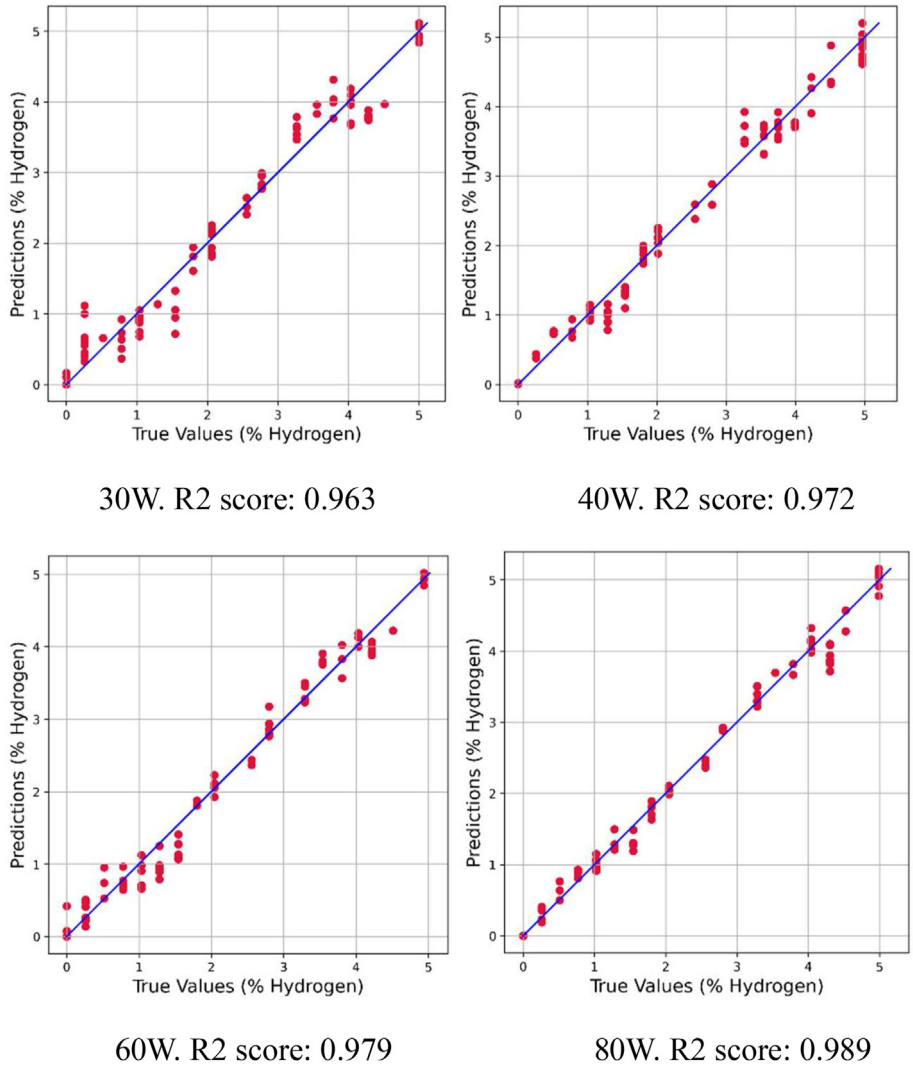

Fig. 10 – Hydrogen content prediction of the residual model when trained with spectral data obtained at RF powers of (30,40,60 and 80w). Higher plasma power seems to result in spectral data that bear features for more efficient model learning and better test predictions results with 30w of RF plasma performing poorest.

characteristics of methane hence why this situation poses a potential challenge for the deep learning model.

But at the same time, ambient moisture (water), is a molecule comprised of two hydrogen atoms and an oxygen atom. As such a valid question may arise as to whether the presence of moisture can influence the learning curve of the deep learning model during training. In our experiments we did not manipulate the moisture content of the air that was fed through the MFC into the plasma. Hence, the moisture content was that of the ambient in the time of data collection. Table 1 illustrates the minimum and maximum humidity of the ambient air obtained from (http://nw3weather.co.uk/) for the 5 days of data capture (see Table 2).

In an RF (radiofrequency) plasma, water molecules (H2O) can undergo various processes and reactions due to the high energy environment. Here are some of the processes that can occur to water molecules in an RF plasma [60].

1). Dissociation: The high energy of the plasma can cause water molecules to dissociate into their constituent atoms:

$$H2O \rightarrow H + OH$$

2). Ionization: Water molecules can also undergo ionization, producing ions:

$$H2O \rightarrow H2O+ + e-$$

3). Excitation: Water molecules may become excited, leading to higher energy states:

$$H2O + \text{energy} \rightarrow \text{Excited State } H2O$$

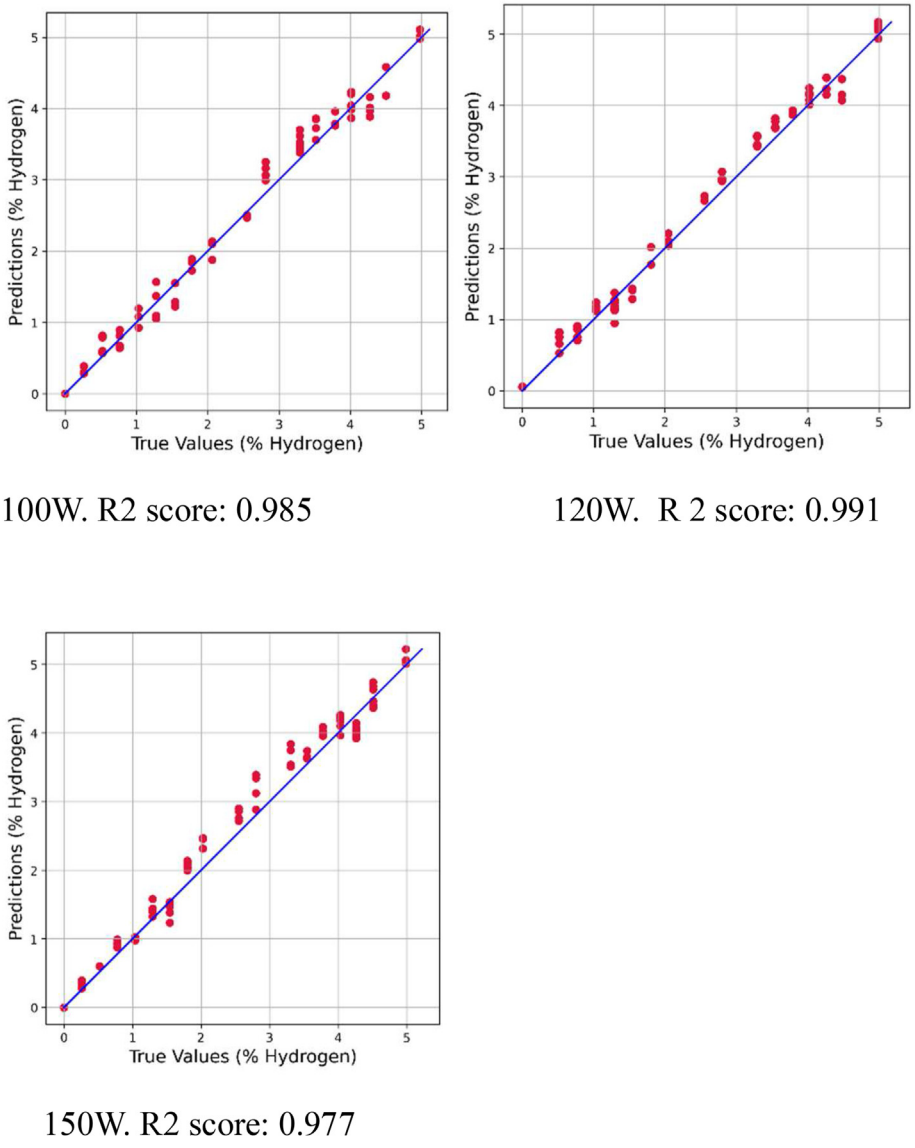

Fig. 11 – Hydrogen content prediction of the residual model when trained with spectral data obtained at RF powers of (100,120 and 150w). The best training and test result predictions occurs at 120w ofplasma powe.

4). Chemical Reactions: Water molecules can participate in chemical reactions with other species present in the plasma. For example, they may react with ions or radicals to form new compounds.
5). Hydrogen and Oxygen Production: In a hydrogen-rich RF plasma, water can be a source of hydrogen (H2) and oxygen (O2) production through dissociation.
6). Radical Formation: Water molecules can break into hydroxyl radicals (OH) and hydrogen radicals (H) through dissociation and subsequent reactions.

Considering the above statements, we can see that when moisture is present, there will be traces of hydrogen present in the plasma as well as hydroxyl radicals even when there is no hydrogen being fed into the plasma during data collection. As such, we can assume that during training, we train the AI model with a given hydrogen quantity (the quantity we feed into the system) while simultaneously the hydrogen generated via water molecule break down is neglected by the model during its training. This is in fact a potential source of error being introduced into the data. Consequently, the model is trained with an inherent error in its learning process. However, this error does not seem to have improvised the model's accuracy as the presence of methane has.

We think, this can be explained as follows.

a. During the 5 days that we have been collecting the spectral data, the average ambient moisture levels have been very similar. If significant moisture variations existed, the effect of this error would be significantly pronounced.
b. Considering that during all the plasma conditions, a certain amount of hydrogen generated from the moisture

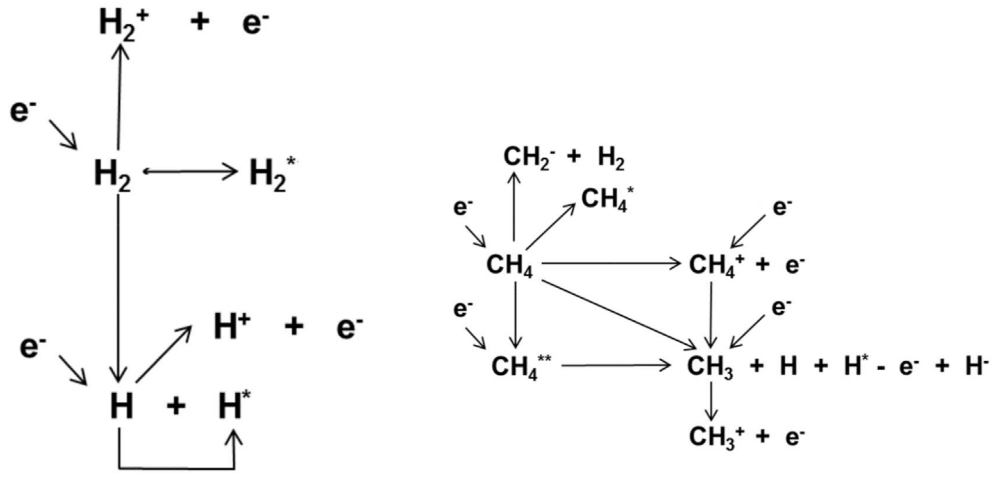

Fig. 12 – A basic representation of species presents in hydrogen and methane plasma. While hydrogen presence in plasma can lead to limited possible species, a methane plasma can have much more complex set of species forming including isolated hydrogen species.

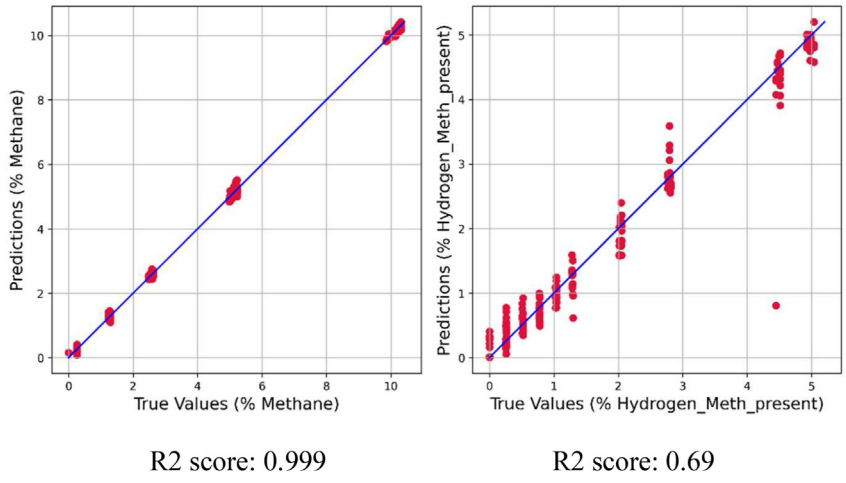

Fig. 13 – Predictions made by the residual CNN model on methane content in air while hydrogen is also present (left). Prediction of hydrogen content while methane is present. While the system is capable of calculating methane content to a high precision from the spectral data it lacks desired accuracy for predicting hydrogen content.

has been present, the spectral features associated to that level of hydrogen content has been captured by the model and during training that background hydrogen has been associated with zero content hydrogen during model's neural weight assignment. Hence, the natural hydrogen arising from break down of the moisture in the plasma is set to a zero benchmark in the model's calculation black box.

c. Unlike moisture which has been present in every single spectral feature within an average threshold described in Table 1, the methane has only been present in certain number of spectral data and as such the model does not associate methane spectral features to be a bench mark of any form, hence when calculating hydrogen content, it is improvised by the methane presence.

However, in future experiments, ambient air drying should be considered and comparison of results with undried air should yield significantly better perspective of developing this concept into maturation.

4.4. *Overall assessment*

This conceptual technology is currently at its infant stage and what has been reported here has been an exploration of this methodology's potential. If it is to be assessed in its current form, one can argue that it will be an expensive solution while the methane interference with hydrogen needs to be resolved. Table two demonstrates a comparison of this technology with the available technologies in the market. The % content reflected in this report, for simplicity represent % flow rate

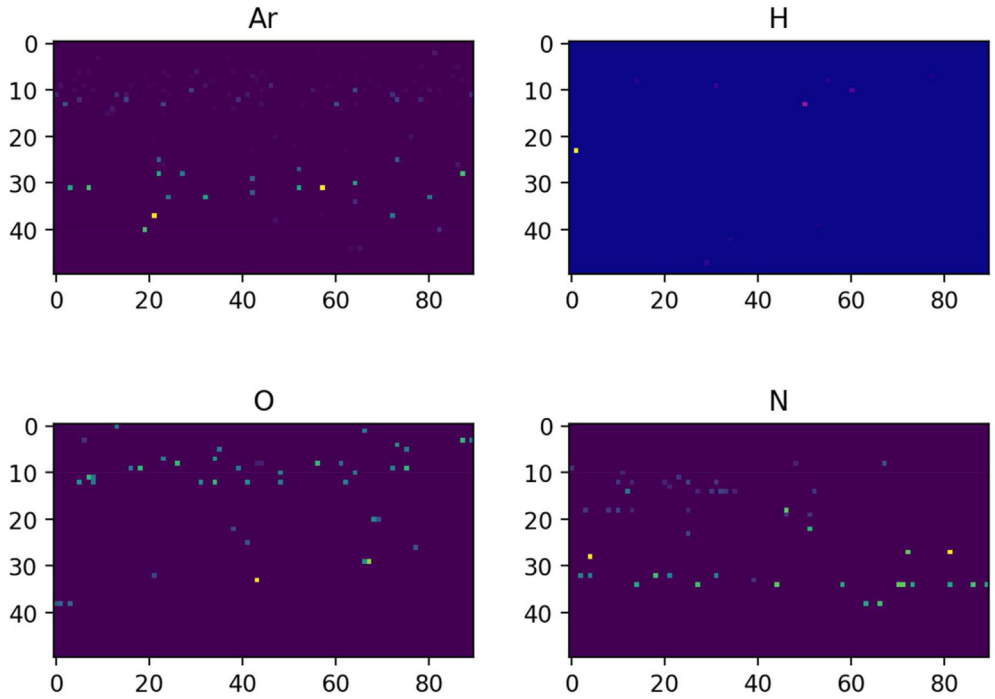

Fig. 14 – Atomic spectra emission wavelengths (strong lines) associated with various electronic transitions were extracted from NIST dataset and converted into a 2D tensor for visualisation. Here we see the transitions for hydrogen (H), argon (Ar), oxygen (O) and nitrogen (N). Hydrogen has lowest number of features. Only emission wavelengths between 200 nm and 1110 nm are included here.

Tabel. 1 – Data associated with ambient humidity in the region where data was collected over a 5-day period.

Measure	Value (anomaly)	Time	Month cumul.	Record High	Record Low
Minimum Humidity	54%	14:55	52%	85%, 2021	34%, 2018
Maximum Humidity	90%	05:25	87%	94%, 2012	69%, 2014
Mean Humidity	71%		70%	88%, 2021	51%, 2014
Minimum Humidity	42%	16:45	51%	72%, 2016	31%, 2010
Maximum Humidity	91%	05:57	87%	97%, 2013	73%, 2017
Mean Humidity	70%		70%	80%, 2016	56%, 2018
Minimum Humidity	45%	13:19	50%	74%, 2019	34%, 2015
Maximum Humidity	85%	05:47	87%	94%, 2019	68%, 2017
Mean Humidity	63%		70%	85%, 2019	52%, 2017
Minimum Humidity	56%	14:41	51%	79%, 2021	29%, 2010
Maximum Humidity	82%	23:59	87%	94%, 2009	79%, 2015
Mean Humidity	69%		70%	87%, 2021	55%, 2010
Minimum Humidity	56%	14:41	51%	79%, 2021	29%, 2010
Maximum Humidity	82%	23:59	87%	94%, 2009	79%, 2015
Mean Humidity	69%		70%	87%, 2021	55%, 2010

From the table we can see slight variation in humidity over the span of the days where we collected our data.

(square cubic centimetre per minute 'sccm') of gasses into the plasma and not ppm figure as the initial objective has been to explore the feasibility of the technique presented in the manuscript.

The minimum and maximum dilutions we have been able to perform with, are dependent on our source gases concentration and the Min/Max flow rate possible with the MFC controller with minimum of 0.1 sccm flow rate.

In our initial studies which this report is related to, the minimum methane or hydrogen content in parts per million we could admit into the plasma to take measurements were about 1400 parts per million (ppm). While this may sound high, as this technology is at an early stage, our initial objective was focused on the experimental set up and constructing a suitable model capable of being able to capture features from the plasma. However, future work will require experiments with significant tly low part per million or part per billion figures. As such the limit of detection via this technique can not be confirmed with confidence until further exploration.

Table 2 – A snapshot comparative evaluation of the existing detector technologies and the concept model proposed in this report.

Technology	Low cost	Stability	Wide Range	Easy build	Fast response	Size	High Sensitivity	High temp Operation	Major disadvantage
Thermal	✔	✔		✔	✔				Sensitive to interfering gases and can damage easily
Electrochemical							✔	✔	Costly and low life
Resistive	✔				✔		✔	✔	Requires oxygen, High cross sensitivity, poor selectivity
Work function	✔				✔	✔	✔		Severe hysteresis losses, drift, and saturation at low gas concentrations
Mechanical						✔			Very hard to fabricate and maintain
Optical		✔			✔		✔		Very cross sensitive with other gases
Acoustic			✔		✔		✔		Sensitive to ambient sound
Catalytic		✔							Slow response, cross interference with other gases
Triboelectric		✔			✔				Hard to manufacture
Plasma AI (Reported here)		✔		✔	✔		✔	✔	Interference with Methane. Expensive, at early at experimental stage. Uncertain limit of detection.

5. Conclusion

While further fine-tuning and adjustments are still required to perfect the hydrogen sensing capability of the concept described here, it clearly demonstrates its potential as a hydrogen detection system, provided that no methane presence is considered. Achieving this ambition will necessitate additional adjustments to the plasma parameters, chamber configuration, collimator design, and more extensive data collection and model training.

While this system can serve as an ideal methane detection system even in the presence of hydrogen, addressing certain challenges is essential for it to operate as a dual Hydrogen/Methane sensing concept. These challenges may be associated with hardware design or may involve delving into the image processing aspect of the concept, such as selective image analysis, focusing on regions uniquely associated with hydrogen.

In terms of application, based on our observations and assessments, rather than being limited to safety leak detection, this system may be considered as a hydrogen production monitoring tool in the process of methane formation or hydrolysis for hydrogen production, achieved by analyzing the reaction outputs. In fact, this exploration will be the authors' focus from this point forward.

Declaration of competing interest

The authors declare that they have no known competing financial interests or personal relationships that could have appeared to influence the work reported in this paper.

REFERENCES

[1] Maksymov IS, Kostylev M. Magneto-electronic hydrogen gas sensors: a critical review. Chemosensors 2022;10:4.
[2] Hacker V, Mitsushima S. Fuel cells and hydrogen: from fundamentals to applied research. Amsterdam, The Netherlands: Elsevier; 2018.
[3] Corbo P, Migliardini F, Ottorino O. Hydrogen fuel cells for road vehicles. Berlin, Germany: Springer; 2011.
[4] Tarhan C. A study on hydrogen, the clean energy of the future: hydrogen storage methods. 2021.
[5] Hübert T, Boon-Brett L, Palmisano V, Bader MA. Developments in gas sensor technology for hydrogen safety. Int J Hydrogen Energy 2014;39:20474–83.
[6] Buttner WJ, Post MB, Burgess R, Rivkin C. An overview of hydrogen safety sensors and requirements. Int J Hydrogen Energy 2011;36:2462–70.
[7] Chang C-H, Lin K-W, Lu H-H, Liu R-C, Liu W-C. Hydrogen sensing performance of a Pd/HfO2/GaOx/GaN based metal oxide-semiconductor type Schottky diode. Int J Hydrogen Energy 2018;43:19816–24.
[8] Podlepetsky B, Nikiforova M, Kovalenko A. Chip temperature influence on characteristics of MISFET hydrogen sensors. Sensor Actuator B Chem 2018;254:1200–5.
[9] Behzadi pour G, Fekri aval L. Highly sensitive work function hydrogen gas sensor based on PdNPs/SiO2/Si structure at room temperature. Results Phys 2017;7:1993–9.
[10] Xu B, Li P, Wang DN, Zhao C, Dai J, Yang M. Hydrogen sensor based on polymer-filled hollow core fiber with Pt-loaded WO3/SiO2 coating. Sensor Actuator B Chem 2017;245:516–23.
[11] Karker NA, Carpenter MA. High figure of merit hydrogen sensor using multipolar plasmon resonance modes. Sensor Actuator B Chem 2017;252:385–90.
[12] Hwang K, T-raissi A, Qin N. Effect of pigment concentration and particle size of TiO2 support on performance of

chemochromic hydrogen tape sensor. Int J Hydrogen Energy 2018;43:9877–83.
[13] Kim YK, Hwang SH, Jeong SM, Son KY, Lim SK. Colorimetric hydrogen gas sensor based on PdO/metal oxides hybrid nanoparticles. Talanta 2018;188:356–64.
[14] Abdalwareth A, Flachenecker G, Angelmahr M, Schade W. Optical fiber evanescent hydrogen sensor based on palladium nanoparticles coated Bragg gratings. Sensor Actuator Phys 2023;361:114594.
[15] Wang J, Dai J, Hu W, Zhang F, Yang M. Improved performance of fiber-optic hydrogen sensor of porous Pt/WO3 based on ZIF-8. Int J Hydrogen Energy 2023. https://doi.org/10.1016/j.ijhydene.2023.06.080.
[16] Abdalwareth A, Flachenecker G, Angelmahr M, Schade W. Optical fiber evanescent hydrogen sensor based on palladium nanoparticles coated Bragg gratings. Sensor Actuator Phys 2023;361:114594.
[17] Simon I, Arndt M. Thermal and gas-sensing properties of a micromachined thermal conductivity sensor for the detection of hydrogen in automotive applications. Sensor Actuator Phys 2002;97–98:104–8.
[18] Tardy P, Coulon JR, Lucat C, Menil F. Dynamic thermal conductivity sensor for gas detection. Sensor Actuator B Chem 2004;98:63–8.
[19] Occelli C, Fiorido T, Perrin-Pellegrino C, Seguin J-L. Sensors for anaerobic hydrogen measurement: a comparative study between a resistive PdAu-based sensor and a commercial thermal conductivity sensor. Int J Hydrogen Energy 2023;48(46):17729–41.
[20] Berndt D, Muggli J, Wittwer F, Langer C, Heinrich S, Knittel T, Schreiner R. MEMS-based thermal conductivity sensor for hydrogen gas detection in automotive applications. Sensor Actuator Phys 2020;305:111670.
[21] Hashtroudi H, Atkin P, Mackinnon IDR, Shafiei M. Low-operating temperature resistive nanostructured hydrogen sensors. Int J Hydrogen Energy 2019;44(48):26646–64.
[22] Mirzaei A, Yousefi HR, Falsafi F, Bonyani M, Lee J-H, Kim J-H, Kim HW, Kim SS. An overview on how Pd on resistive-based nanomaterial gas sensors can enhance response toward hydrogen gas. Int J Hydrogen Energy 2019;44(36):20552–71.
[23] Lo C, Tan S-W, Wei C-Y, Tsai J-H, Lour W-S. Sensing properties of resistive-type hydrogen sensors with a Pd–SiO2 thin-film mixture. Int J Hydrogen Energy 2013;38(1):313–8.
[24] Sanger A, Kumar A, Kumar A, Chandra R. Highly sensitive and selective hydrogen gas sensor using sputtered grown Pd decorated MnO2 nanowalls. Sensor Actuator B Chem 2016;234:8–14.
[25] Chauhan PS, Bhattacharya S. Vanadium pentoxide nanostructures for sensitive detection of hydrogen gas at room temperature. Journal of Energy and Environmental Sustainability 2017;2:69–74.
[26] Chauhan PS, Kant R, Rai A, Gupta A, Bhattacharya S. Facile synthesis of ZnO/GO nanoflowers over Si substrate for improved photocatalytic decolorization of MB dye and industrial wastewater under solar irradiation. Mater Sci Semicond Process 2019;89:6–17.
[27] Gong J, Wang Z, Tang Y, Sun J, Wei X, Zhang Q, Tian G, Wang H. MEMS-based resistive hydrogen sensor with high performance using a palladium-gold alloy thin film. J Alloys Compd 2023;930.
[28] Wang Z, Huang S, Men G, Han D, Gu F. Sensitization of Pd loading for remarkably enhanced hydrogen sensing performance of 3DOM WO3. Sensor Actuator B Chem 2018;262:577–87.
[29] Park JH, Ko JH, Hong S, Shin YJ, Park N, Kang S, et al. Hollow and microporous Zn Porphyrin networks: outer shape dependent ammonia sensing by quartz crystal microbalance. Chem Mater 2015;27:5845–8.
[30] Yang M, He J. Graphene oxide as quartz crystal microbalance sensing layers for detection of formaldehyde. Sensor Actuator B Chem 2016;228:486–90.
[31] Devkota J, Mao E, Greve DW, Ohodnicki PR, Baltrus J. A surface acoustic wave hydrogen sensor with tin-doped indium oxide layers for intermediate temperatures. Sensor Actuator B Chem 2022;354:131229.
[32] Ha NH, Nam NH, Dung DD, Phuong NH, Thach PD, Hong HS. (2017). Hydrogen gas sensing using palladium-graphene nanocomposite material based on surface acoustic wave. J Nanomater 2017:1–6.
[33] Kerroum I, Fall ME, Reinhardt A, Domingue F. Hydrogen effect on density and Young's modulus of thin films in acoustic sensors. Sensor Actuator B Chem 2016;223:520–6.
[34] Rýger I, Vanko G, Lalinský T, Haščík Š, Benčúrová A, Nemec P, Andok R, Tomáška M. GaN/SiC based surface acoustic wave structures for hydrogen sensors with enhanced sensitivity. Sensor Actuator Phys 2015;227:55–62.
[35] Perez-Cortes L, Hernandez-Rodriguez C, Mazingue T, Lomello-Tafin M. Functionality of Surface Acoustic Wave (SAW) transducer for palladium–platinum-based hydrogen sensor. Sensor Actuator Phys 2016;251:35–41.
[36] Basu AK, Sarkar H, Bhattacharya S. Fabrication and resilience measurement of thin aluminium cantilevers using scanning probe microscopy. Proceedings of the 3rd International Conference on Foundations and Frontiers in Computer, Communication and Electrical Engineering (C2E2 - 2016) 2016;1813:457–60.
[37] Iannuzzi D, Slaman M, Rector JH, Schreuders H, Deladi S, Elwenspoek MC. A fiber-top cantilever for hydrogen detection. Sensor Actuator B Chem 2007;121:706–8.
[38] Baselt DR, Fruhberger B, Klaassen E, Cemalovic S, Britton CL, Patel SV, et al. Design and performance of a microcantilever-based hydrogen sensor. Sensor Actuator B Chem 2003;88:120–31.
[39] Li H, Li Y, Wang K, Lai L, Xu X, Sun B, Yang Z, Ding G. Ultra-high sensitive micro-chemo-mechanical hydrogen sensor integrated by palladium-based driver and high-performance piezoresistor. Int J Hydrogen Energy 2021;46(1):1434–45.
[40] Kim M-O, Lee K, Na H, Kwon D-S, Choi J, Lee J-I, Baek D-H, Kim J. Highly sensitive cantilever type chemo-mechanical hydrogen sensor based on contact resistance of self-adjusted carbon nanotube arrays. Sensor Actuator B Chem 2014;197:414–21.
[41] Wang C, Yang J, Li J, Luo C, Xu X, Qian F. Solid-state electrochemical hydrogen sensors: a review. Int J Hydrogen Energy 2023;48(80):31377–91.
[42] Alemayehu D, Bitew Z, Yohannes YB. Development of a new electrochemical sensor based on nafion/cobalt-doped bismuth ferrite nanoparticle modified glassy carbon electrode for detection of hydrogen peroxide. Sensing and Bio-Sensing Research 2023:100586.
[43] Kim S, Song Y, Ahn H-J, Jeong H-M, Yoo BU, Lee J-Y. Ultrafast response/recovery and high sensitivity of a hydrogen gas sensor at room temperature based on electrochemically deposited Sb2Te3/polystyrene composite film. Int J Hydrogen Energy 2023. https://doi.org/10.1016/j.ijhydene.2023.08.092.
[44] Jayanthi E, Murugesan N, Suneesh AS, Ramesh C, Anthonysamy S. Sensing behavior of room temperature amperometric H2 sensor with Pd electrodeposited from ionic liquid electrolyte as sensing electrode. J Electrochem Soc 2017;164:H5210–7.
[45] Lin L, Zeng X. Toward continuous amperometric gas sensing in ionic liquids: rationalization of signal drift nature and calibration methods. Anal Bioanal Chem 2018;410:4587–96.
[46] Korotcenkov G, Han SD, Stetter JR. Review of electrochemical hydrogen sensors. Chem Rev 2009;109:1402–33.

[47] Chauhan PS, Bhattacharya S. Hydrogen gas sensing methods, materials, and approach to achieve parts per billion level detection: a review. Int J Hydrogen Energy 2019;44(47):26076–99.
[48] Advanced Materials Research Vols 774-776 (2013) pp 471-478, (2013) Trans Tech Publications, Switzerland. DOI: 10.4028/www.scientific.net/AMR.774-776.471.
[49] Jin D-Z, Yang Z-H, Tang P-Y, Xiao K, Dai J-Y. Hydrogen plasma diagnosis in penning ion source by optical emission spectroscopy. Vacuum 2009;83:451–3.
[50] Drawin HW, Emard F. Instantaneous population densities of the excited levels of hydrogen atoms, hydrogen-like ions and helium atoms in optically thin and thick non-LTE plasmas. 1970. Report EUR-CEA-FC-534.
[51] Fantz U, Falter HD, Franzen P, Speth E. Rev Sci Instrum 2006;77:03A516.
[52] Johnson LC, Hinnov EJ. Quantum Spectroscopy and Radiative Transfer 1973;13:333.
[53] Chen CK, Wei T, Collins LR, et al. J Phys Appl Phys 1999;32:688–98.
[54] Sawada K, Fujimoto T. J Appl Phys 1995;78(5):2913–24.
[55] Mantzaris NV, Gogolides E, Boudouvis AG. Plasma Chem Plasma Process 1996;16(3):301–27.
[56] Morgan WL. Plasma Chem Plasma Process 1992;12(4).
[57] Petrov GM, Giuliani JL. J Appl Phys 2001;90(2).
[58] He K, Zhang X, Ren S, Sun J. (2016). Deep residual learning for image recognition. In: Proceedings of the IEEE conference on computer vision and pattern recognition (CVPR), Las Vegas, NV, USA; 27–30 June 2016. p. 770–8.
[59] NIST atomic spectra database. https://physics.nist.gov/PhysRefData/ASD/lines_form.html (Accessed: 1 August 2023).
[60] Nguyen SVT, Foster JE, Gallimore AD. Operating a radio-frequency plasma source on water vapor. Rev Sci Instrum 2009;80(8):083503.